Boosting the Performance of BiVO 4 Prepared through Alkaline Electrodeposition with an Amorphous Fe Co-catalyst

Hiba Saada, Rawa Abdallah, Bruno Fabre, Didier Floner, Stéphanie Fryars, Antoine Vacher, Vincent Dorcet, Cristelle Mériadec, Soraya Ababou-Girard, Gabriel Loget

Boosting the performance of $BiVO_4$ prepared by alkaline electrodeposition with an amorphous Fe co-catalyst

Hiba Saada,[a,b] Rawa Abdallah,[b] Bruno Fabre,[a] Didier Floner,[a] Stéphanie Fryars,[a] Antoine Vacher,[a] Vincent Dorcet,[a] Cristelle Meriadec,[c] Soraya Ababou-Girard,[c] Gabriel Loget*[a]

Abstract: $BiVO_4$ is a very promising *n*-type semiconductor for water-splitting photoelectrochemical cells. We report here a new method to prepare $BiVO_4$ photoanodes that is based on an alkaline electrodeposition process that avoids chemical etching of Bi. In addition, we present a simple and general method to prepare amorphous coatings of FeO_x that behaves as a co-catalyst on our $BiVO_4$ material, improving the water splitting photocurrent.

The conversion of renewable energies into energy-rich fuels that can be stored, transported and used to generate electricity on-site and on-demand is a very attractive way to solve the main problem of renewables, namely their intermittency.[1] In this frame, water-splitting photoelectrochemical cells (PECs) are attracting a considerable amount of attention.[2–5] These devices are made of semiconductor (SC) photoelectrodes that are able to convert solar energy into H_2 (an energy-rich fuel) and O_2. Upon light absorption, the charge carriers photogenerated in the SC are driven to the solid-liquid interface where they participate to the water splitting half-reactions: hydrogen evolution reaction (HER) and oxygen evolution reaction (OER).[2–5] In this process, the OER is the most challenging reaction as it requires a considerable energy input[6] and also because most of SCs are subject to photocorrosion, which makes them unstable in photoelectrolysis conditions.[7] Among *n*-type SCs that have been investigated as photoanodes for OER, $BiVO_4$ stands out for several reasons:[8],[9] first, it is composed of relatively abundant and non-toxic materials,[10] it has a bandgap narrow enough (2.4 eV) to absorb a significant part of the solar spectrum,[11] a valence band below the O_2/H_2O standard potential and a theoretical solar-to-hydrogen efficiency of ~9%.[12] However, the water splitting performance of $BiVO_4$ is still limited by its poor charge extraction[13] and its low catalytic activity for OER, which implies to employ additional chemical and surface engineering processes to improve its efficiency.[14] Among these methods, $BiVO_4$ doping[15,16] photocharging[17,18] cathodic polarization,[19] nanostructuration,[20,21] as well as its interfacing with: highly active OER co-catalysts (*cocats*)[22–25] another SC[26–29] and plasmonic materials[30,31] have shown great promise. The synthesis of photoelectrochemically active $BiVO_4$ on a conductive substrate is thus of great importance and can be performed by: *i*) spray-based,[13,18,29] or *ii*) hydrothermal[17,19] methods, *iii*) metal-organic decomposition,[21,28,30] *iv*) physical vapor deposition[26,32] and *v*) electrodeposition.[22,33–36] The latter approach is very attractive due to its simplicity and its low cost[37,38] and electrodeposited $BiVO_4$ has already led to very important breakthroughs.[22,25] Furthermore, electrodeposition processes are generally easily tunable and can be applied to various types of conductive substrates, regardless their composition and geometry, which is particularly adapted for $BiVO_4$ morphological engineering.[20,21] So far, the great majority of works devoted to electrodeposited $BiVO_4$ employed the electrodeposition processes reported by Choi *et al.*[22,33,34] and all used organic[34] or acid electrolytes[22,33,35] to ensure the solubility of Bi^{3+}. However, acidic media can be detrimental because Bi^0 is soluble at low pH[39] and acid electrolytes are known to deteriorate the Bi-substrate interaction (Figure S1),[34] in addition, several substrates are incompatible with low pH electrochemical treatments.[40–42] In this article, we report the first fabrication process based on alkaline electrodeposition to generate $BiVO_4$ and we introduce a new OER-active Fe-based amorphous *cocat* to boost considerably its photoelectrochemical performance.

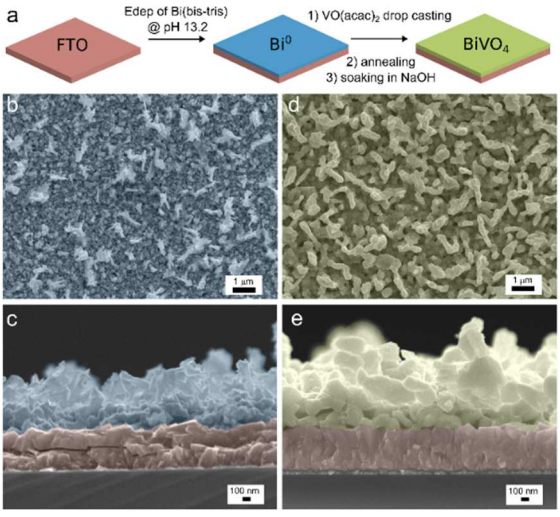

Figure 1. a) Scheme showing the preparation process. b-e) Colored SEM images showing top views (b,d) and cross-sections (c,e) of Bi (b,c) and $BiVO_4$ (d,e) layers on FTO. In these images, Bi was colorized in blue, $BiVO_4$ in green and FTO in red.

[a] H. Saada, Dr. D. Floner, Dr. B. Fabre, S. Fryars, Dr. A. Vacher, Dr. V. Dorcet, Dr. G. Loget
Univ Rennes, CNRS, ISCR (Institut des Sciences Chimiques de Rennes) UMR6226-ScanMAT, F-35000 Rennes, France.
Email: gabriel.loget@univ-rennes1.fr

[b] Dr. Rawa Abdallah
Lebanese University, EDST, Azm Center for Research in Biotechnology and Its Applications, Laboratory of Applied Biotechnology, LBA3B, El Mitein Street, Tripoli, Lebanon

[c] C. Meriadec, Dr. S. Ababou-Girard
Univ Rennes, CNRS, IPR (Institut de Physique de Rennes)-UMR6251, F-35000 Rennes, France.

Supporting information for this article is given via a link at the end of the document.

Our strategy (**Figure 1a**) consisted in first electroplating Bi^0 on fluorine-doped SnO_2 (FTO) and then converting it to $BiVO_4$. The first problem for electrodepositing Bi at high pH is to solubilize the Bi source. Indeed; common Bi^{3+} salts are only soluble at low pH whereas at high pH they hydrolyze and precipitate as oxides and hydroxides. We thus employed a stable 1:1 Bi^{3+}: 2,2-bis(hydroxymethyl)-2,2',2''-nitriloethanol (bis-tris) complex that was synthesized by mixing bis-tris with Bi_2O_3 in strongly basic conditions. Note that bis-tris is a widely available commercial compound, usually employed for the preparation of biological buffers.[43,44] Bi(bis-tris) was totally soluble in highly alkaline conditions and was employed as the Bi source in the electrodeposition bath, that also contained 0.1 M NaOH to maintain the high alkalinity (measured pH = 13.2). Electrodeposition was carried out by applying 500 successive 2 s-long galvanostatic pulses of -0.5 $mA.cm^{-2}$ spaced by a rest time of 1 s in order to resupply the liquid interface with Bi(bis-tris). The resulting coatings were dark grey, and, according to scanning electron microscopy (SEM) images (Figure 1b,c), consisted of ~0.7 µm-thick microcrystalline films that covered all the FTO surface (additional SEM pictures are shown in Figure S3). Energy-dispersive X-ray spectroscopy (EDS), performed on a large area, (blue curve in **Figure 2a**, see Figures S3 and S4 for more details) confirmed the presence of Bi and Sn (coming from the underlying FTO surface). In addition, all peaks present in the corresponding X-ray diffraction (XRD) pattern (blue curve of Figure 2b) could be attributed to metal Bi (blue lines, ISCD #64703) and FTO (red lines, ISCD #39178).

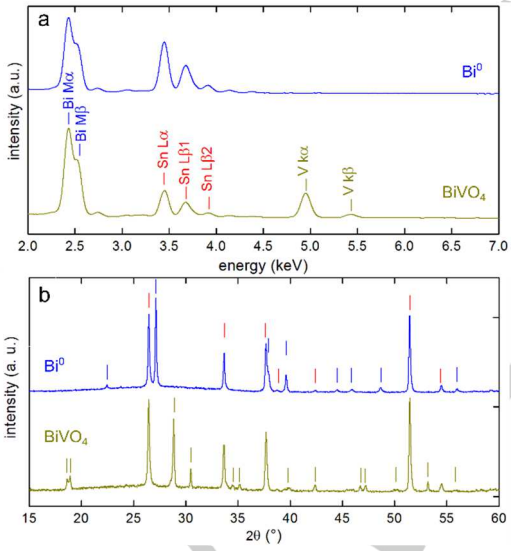

Figure 2. a) EDS spectra of a surface after Bi electrodeposition (blue) and after conversion in $BiVO_4$ (green). b) XRD patterns of a surface after Bi electrodeposition (blue, the blue lines indicate the position of the peaks of ISCD #64703), and after conversion in $BiVO_4$ (green, the green lines indicate the peak position of ISCD #100604) the position of FTO peaks (ISCD #39178) are indicated by red lines.

After electrodeposition, the Bi^0 coatings were converted in $BiVO_4$ by a simple two-step process that consisted in drop-casting a solution of vanadyl acetylacetonate ($VO(acac)_2$) and annealing the surface in air at 500 °C for 2 h, as described in previous works.[34] During this treatment, V diffused inside the Bi film which oxidized to generate $BiVO_4$. The excess V_2O_5 was finally dissolved by soaking the surfaces in 1 M NaOH for 30 min. This treatment converted the Bi coatings to yellow, ~1.1 µm-thick rough and homogeneous films (Figure 1d,e and Figure S6). EDS (green curve in Figure 2a, see Figures S6 and S7 for more details) confirmed the incorporation of V in the coating with a calculated Bi to V atomic ratio of 1.0 (Table S1). Moreover, XRD (green curve in Figure 2b) revealed the total disappearance of the Bi^0 peaks and the apparition of new peaks, which can all be attributed to monoclinic $BiVO_4$ (green lines). These results demonstrate that $BiVO_4$ layers can be prepared *via* alkaline electrodeposition of Bi. Now, we introduce a general method to immobilize a Fe-based *cocat* on various substrates that will be applied to our $BiVO_4$ material.

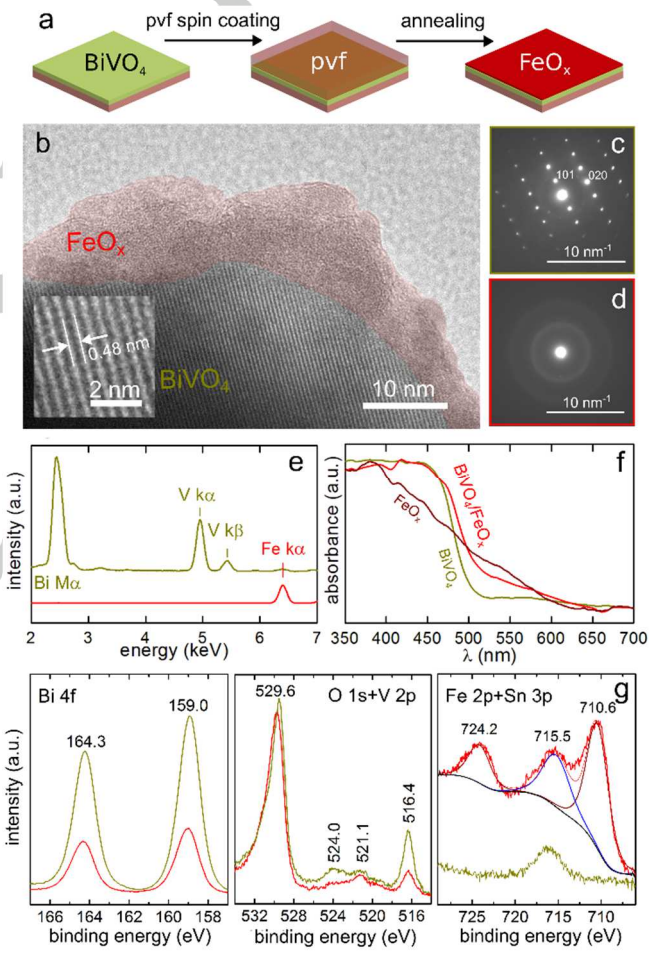

Figure 3. a) Scheme showing the modification process on $BiVO_4$. b) Colored HR TEM image showing the $BiVO_4$ (grey)/FeO_x (red) interface. Inset: high magnification image showing the spacing of the (101) planes in $BiVO_4$. c,d) Indexed SAED patterns and e) corresponding EDS spectra recorded on a $BiVO_4$ particle [(c) and green curve in (e)] and on a Fe-rich area [(d) and red curve in (e)]. f) Normalized absorbance spectra for $BiVO_4$, FeO_x, and $BiVO_4/FeO_x$. g) XPS spectra showing the Bi 4f (left), the O 1s and V 2p (middle) and the Fe 2p and Sn 3p (right) areas before (green) and after (red) modification with FeO_x, including Fe 2p fits (brown line), Sn 3p fit (blue line), background (black line) and fitting envelope (thin red line).

Fe oxides and hydroxides are promising OER *cocats* for solar fuel systems[6] and Fe has a very low market price,[10] which encouraged us to develop a method to coat Fe oxides on conducting and SC materials. Our process is very simple (**Figure 3a**) and consists in spin coating a dimethylformamide (DMF) solution containing a soluble commercial Fe-containing polymer, poly(vinylferrocene) (pvf) (shown in Figure S2), and annealing the substrate at a low temperature (300 °C) to generate an OER-active Fe-based *cocat* layer.

SEM did not allow to observe a difference of morphology before and after modification but transmission electron microscopy (TEM) clearly revealed the presence of two distinct phases (Figure 3b). The first one was $BiVO_4$, as indicated by its composition (green curve of Figure 3e, Bi to V ratio of 1) and by the agreement between the selected area electron diffraction (SAED) pattern (Figure 3c) and the structure of this phase (ICSD #100604). The second phase, colored in red in Figure 3b, was amorphous (Figure 3b,d) and contained a high content of Fe (red curve of Figure 3e) resulting from the thermal decomposition of the pvf film on $BiVO_4$ during annealing. As shown in Figure 3b (additional TEM images are shown in Figure S9), this phase was often observed at the edge of the $BiVO_4$ particles, showing that our treatment produced a discontinuous few nm-thick amorphous film over the $BiVO_4$ layer. In addition, X-ray photoelectron spectroscopy (XPS) performed on bare and coated $BiVO_4$ surfaces confirmed the presence of the expected elements (Bi, V, and O), as well as Sn originating from the FTO substrate (Figure S10). After modification, the intensity of the Bi $4f_{7/2}$ and $4f_{5/2}$ bands (Figure 3g), respectively located at 159.0 and 164.3 eV and the V $2p_{3/2}$ and $2p_{1/2}$, at 516.4 and 524.0 eV, decreased (note the O 1s satellite peak at 521.1 eV), well in line with the presence of a coating on the outer $BiVO_4$ surface. More interestingly, new bands at 710.6 and 724.2 eV appeared after modification, which fit very well with the Fe $2p_{3/2}$ and $2p_{1/2}$, of oxidized Fe species.[45] In contrast, Fe $2p_{3/2}$ values for carbonated compounds such as ferrocene, $Fe(CO_3)$ and $Fe(CO)_5$ are commonly found at lower binding energies (707.5 eV for ferrocene, 709.4 eV $Fe(CO)_5$ and 710.2 eV for $Fe(CO_3)$).[45,46] If residual carbon, originating from pvf decomposition, is expected to be present in the amorphous phase, its presence did not influence the C 1s region (Figure S11). Besides, due to the similitude of XPS spectra of FeO, Fe_3O_4 and Fe_2O_3,[45] the precise stoichiometry of the formed Fe oxide could not be determined. To conclude, these results demonstrate that the amorphous phase contained Fe that was mainly present in the form of an oxide, thus, for sake of simplicity, we refer to this layer as FeO_x (with $1 < x < 1.5$). The optical properties of the samples were analyzed by absorbance measurements (Figure 3f). The sample before modification exhibited the typical profile for monoclinic $BiVO_4$ (green curve),[35] with an optical band gap of 2.5 eV (Figure S12a). The sample modified with FeO_x (red curve) displayed an enlarged absorption window with a shoulder in the visible range (up to 650 nm), that was attributed to the deposited FeO_x, if one refers to the spectrum of a bare FeO_x film showing an absorption in this spectral window (brown curve).

In order to evaluate the beneficial effects of the FeO_x, non-photoactive surfaces, such as FTO and carbon paper (C_{pap}), were first modified with amorphous FeO_x and then tested for OER at a moderate pH (K-borate buffer, pH = 9.6). The cyclic voltammetry (CV) results clearly indicate that, in both cases, the presence of FeO_x considerably improved OER as it decreased the onset potential (E_{onset}, here arbitrary set for j = 0.05 mA cm^{-2}) from 100 mV for C_{pap} to 280 mV for FTO and also increased the reaction kinetics, as seen by the higher voltammetric slope after modification (Figure 4a). Next, we applied the method to our $BiVO_4$ photoanodes and tested them for photoelectrochemistry by linear sweep voltammetry (LSV, Figure 4b) under simulated sunlight (AM 1.5G) in the same electrolyte. In the absence of illumination, the measured currents were negligible (dark curves). In contrast, anodic currents were clearly observed upon illumination. Bare $BiVO_4$ (green curve) was photoelectrochemically active but had a low E_{onset} of 0.89 V (all potentials are referred vs. Reversible Hydrogen Electrode RHE) and a sluggish activity, as generally observed for unmodified $BiVO_4$ photoanodes.[14] After coating the photoanode, the activity considerably increased (red curve), as demonstrated by the decreased E_{onset} and the improved fill factor. The performance could be further enhanced by applying a simple cathodic treatment to the photoanode, recently reported by Wang *et al.*,[19] that is expected to create oxygen vacancies on the $BiVO_4$ (see the experimental section for more details). In this case, the photoelectrochemical performance was very close to the benchmark performance obtained for the FeO_x-coated $BiVO_4$ in the presence of a hole acceptor (H_2O_2, dashed red curve). By comparing these two curves, we could estimate a charge transfer efficiency ($\eta_{transfer}$) of 92% at 1.23 V (*vs* 65% for the untreated photoanode, see experimental part for more details).[47] Remarkably, all values of E_{onset} obtained for the FeO_x-coated photoanodes were comprised between 0.3 and 0.4 V, close to that of state-of-the-art $BiVO_4$ photoanodes modified with Fe-based catalysts.[22]

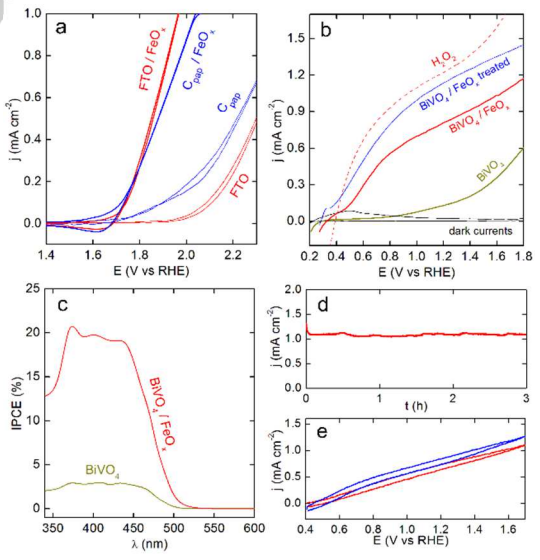

Figure 4. a) CVs showing the anodic behavior of unmodified (thin lines) and FeO_x-coated (thick lines) FTO (red) and carbon paper (blue). b) LSVs recorded in the dark (black full line) or under illumination by simulated sunlight for $BiVO_4$ (green full line), FeO_x-coated $BiVO_4$ (red full line) and FeO_x-coated $BiVO_4$ that was electrochemically treated (blue full line); the LSV of an illuminated FeO_x-coated $BiVO_4$ in the presence of H_2O_2 is also shown (red dashed line). The curves shown in a) and b) were recorded in K-borate buffer (pH = 9.6) at 50 mV s^{-1}. c) IPCE spectra recorded at 1.3 V with a bare $BiVO_4$ and a FeO_x-coated

$BiVO_4$ photoanode. d) CA curve showing the stability of a $BiVO_4/FeO_x$ photoanode held at 1.7 V. e) CVs under illumination before and after the stability test.

The benefit of using the FeO_x coating was also revealed by the incident photon-to-current efficiency (IPCE) spectra (Figure 4c), which showed a considerable enhancement of the photoconversion efficiency for the coated electrode (note that the IPCE decrease at wavelength <370 nm is likely caused by FTO absorption).[41] Interestingly, it can be observed on plots derived from this data (Figures S11b,c) that the photoelectrochemical band gap was, in both cases, equal to the optical band gap (2.5 eV). In addition, because the band gap energy was the same before and after modification, we can conclude that even if FeO_x increased the optical absorbance in the visible spectrum (Figure 3f) it did not dope $BiVO_4$, nor generate electrochemically "active" charge carriers and did not act as a photosensitizer. It rather promoted the extraction of $BiVO_4$ charge carriers and acted as a *cocat*, improving the reaction kinetics. The so-prepared photoanodes were relatively stable and could operate for 3 h (Figure 4d), without any decrease of their voltammetric behavior (Figure 4e). Further SEM (Figure S13) and EDS (Figure S14) analyses carried out after long-term photoelectrolysis confirmed the stability of the material.

In conclusion, we have reported a new method to fabricate photoelectrochemically-active $BiVO_4$. The process is the first one that is based on an alkaline electrodeposition process, which totally avoids chemical etching of Bi and provides a robust substrate-Bi interaction. This process may allow employing materials that are not stable in acidic conditions as $BiVO_4$ substrates and should be useful to design new structures of photoanode. In addition, we have reported a new, simple and versatile method to coat conducting and SC surfaces with a catalytic amorphous layer of FeO_x and we have demonstrated that the resulting FeO_x-coated $BiVO_4$ photoanodes show an enhanced photoelectrocatalytic efficiency. Although the performances of these photoanodes are still lower than the best reported (in the range of 5 mA cm^{-2}) [22] given the simplicity of the reported methods, they should open new possibilities for the preparation of photoelectrochemical cells for the generation of solar fuels.

Acknowledgments

This work was supported by CNRS and Université de Rennes 1. AZM & SAADE Association is fully acknowledged for the financial support. We acknowledge ScanMAT/THEMIS for TEM and F. Gouttefangeas and L. Joanny (ScanMAT/CMEBA) are acknowledged for SEM imaging.

Keywords: bismuth vanadate • iron • electrodeposition • water-splitting • solar fuels

[1] N. S. Lewis, D. G. Nocera, *Proc. Natl. Acad. Sci.* **2006**, *103*, 15729–15735.

[2] A. Rothschild, H. Dotan, *ACS Energy Lett.* **2017**, *2*, 45–51.

[3] K. Sivula, R. van de Krol, *Nat. Rev. Mater.* **2016**, *1*, 15010.

[4] M. R. Shaner, H. A. Atwater, S. Lewis, E. W. Mcfarland, *Energy Environ. Sci.* **2016**, *9*, 2354–2371.

[5] Q. Jing, Z. Wei, C. Rui, *Adv. Energy Mater.* **2017**, *8*, 1701620.

[6] B. M. Hunter, H. B. Gray, A. M. Müller, *Chem. Rev.* **2016**, *116*, 14120–14136.

[7] D. Bae, B. Seger, P. C. K. Vesborg, O. Hansen, I. Chorkendorff, *Chem. Soc. Rev.* **2017**, *46*, 1933–1954.

[8] Y. Park, K. J. McDonald, K.-S. Choi, *Chem. Soc. Rev.* **2013**, *42*, 2321–2337.

[9] H. L. Tan, R. Amal, Y. H. Ng, *J. Mater. Chem. A* **2017**, *5*, 16498–16521.

[10] P. C. K. Vesborg, T. F. Jaramillo, *RSC Adv.* **2012**, *2*, 7933–7947.

[11] M. S. Prévot, K. Sivula, *J. Phys. Chem. C* **2013**, *117*, 17879–17893.

[12] A. F. Fatwa, N. Firet, R. van de Krol, *ChemCatChem* **2012**, *5*, 490–496.

[13] C. Zachaus, F. F. Abdi, L. M. Peter, R. van de Krol, *Chem. Sci.* **2017**, *8*, 3712–3719.

[14] B. Lamm, B. J. Trześniewski, H. Döscher, W. A. Smith, M. Stefik, *ACS Energy Lett.* **2018**, *3*, 112–124.

[15] F. F. Abdi, T. J. Savenije, M. M. May, B. Dam, R. van de Krol, *J. Phys. Chem. Lett.* **2013**, *4*, 2752–2757.

[16] Y. Kuang, Q. Jia, G. Ma, T. Hisatomi, T. Minegishi, H. Nishiyama, M. Nakabayashi, N. Shibata, T. Yamada, A. Kudo, et al., *Nat. Energy* **2016**, *2*, 16191.

[17] T. Li, J. He, B. Peña, C. P. Berlinguette, *Angew. Chem. Int. Ed.* **2015**, *55*, 1769–1772.

[18] B. J. Trzesniewski, I. A. Digdaya, T. Nagaki, S. Ravishankar, I. Herraiz-Cardona, D. A. Vermaas, A. Longo, S. Gimenez, W. A. Smith, *Energy Environ. Sci.* **2017**, *10*, 1517–1529.

[19] S. Wang, P. Chen, J.-H. Yun, Y. Hu, L. Wang, *Angew. Chem. Int. Ed.* **2017**, *56*, 8500–8504.

[20] S. Xiao, C. Hu, H. Lin, X. Meng, Y. Bai, T. Zhang, Y. Yang, Y. Qu, K. Yan, J. Xu, et al., *J. Mater. Chem. A* **2017**, *5*, 19091–19097.

[21] Y. Qiu, W. Liu, W. Chen, W. Chen, G. Zhou, P.-C. Hsu, R. Zhang, Z. Liang, S. Fan, Y. Zhang, et al., *Sci. Adv.* **2016**, *2*.

[22] T. W. Kim, K.-S. Choi, *Science* **2014**, *343*, 990 LP-994.

[23] M. F. Lichterman, M. R. Shaner, S. G. Handler, B. S. Brunschwig, H. B. Gray, N. S. Lewis, J. M. Spurgeon, *J. Phys. Chem. Lett.* **2013**, *4*, 4188–4191.

[24] F. S. Hegner, I. Herraiz-Cardona, D. Cardenas-Morcoso, N. López, J.-R. Galán-Mascarós, S. Gimenez, *ACS Appl. Mater. Interfaces* **2017**, *9*, 37671–37681.

[25] B. Zhang, L. Wang, Y. Zhang, Y. Ding, Y. Bi, *Angew. Chem. Int. Ed.* **2018**, *57*, 2248–2252.

[26] J. Resasco, H. Zhang, N. Kornienko, N. Becknell, H. Lee, J. Guo, A. L. Briseno, P. Yang, *ACS Cent. Sci.* **2016**, *2*, 80–88.

[27] P. M. Rao, L. Cai, C. Liu, I. S. Cho, C. H. Lee, J. M. Weisse, P. Yang, X. Zheng, *Nano Lett.* **2014**, *14*, 1099–1105.

[28] J. H. Kim, J.-W. Jang, Y. H. Jo, F. F. Abdi, Y. H. Lee, R. van de Krol, J. S. Lee, *Nat. Commun.* **2016**, *7*, 13380.

[29] P. Chakthranont, T. R. Hellstern, J. M. McEnaney, T. F. Jaramillo, *Adv. Energy Mater.* **2017**, *7*, 1701515.

[30] Z. Liwu, L. Chia-Yu, V. V. K., R. Erwin, S. Ullrich, J. J. Baumberg,

Small **2014**, *10*, 3970–3978.

[31] K. J. Kyu, S. Xinjian, J. M. Jin, P. Joonsuk, H. H. Soo, K. S. Hyun, G. Yu, H. T. F., F. Shanhui, L. Chang-Lyoul, et al., *Adv. Energy Mater.* **2017**, *8*, 1701765.

[32] Z. Wenrui, Y. Danhua, T. Xiao, L. Mingzhao, *Adv. Funct. Mater.* **2018**, *28*, 1705512.

[33] J. A. Seabold, K.-S. Choi, *J. Am. Chem. Soc.* **2012**, *134*, 2186–2192.

[34] D. Kang, Y. Park, J. C. Hill, K.-S. Choi, *J. Phys. Chem. Lett.* **2014**, *5*, 2994–2999.

[35] S. Wang, P. Chen, Y. Bai, J.-H. Yun, G. Liu, L. Wang, *Adv. Mater.* **2018**, *30*, 1800486.

[36] S. Wang, T. He, J.-H. Yun, Y. Hu, M. Xiao, A. Du, L. Wang, *Adv. Funct. Mater.* **2018**, *28*, 1802685.

[37] D. Kang, T. W. Kim, S. R. Kubota, A. C. Cardiel, H. G. Cha, K.-S. Choi, *Chem. Rev.* **2015**, *115*, 12839–12887.

[38] G. V Govindaraju, G. P. Wheeler, D. Lee, K.-S. Choi, *Chem. Mater.* **2017**, *29*, 355–370.

[39] M. Pourbaix, *Atlas of Electrochemical Equilibria in Aqueous Solutions*, National Association Of Corrosion Engineers, Houston, Tex., **1974**.

[40] N. R. Armstrong, A. W. C. Lin, M. Fujihira, T. Kuwana, *Anal. Chem.* **1976**, *48*, 741–750.

[41] Y. Liang, T. Tsubota, L. P. A. Mooij, R. van de Krol, *J. Phys. Chem. C* **2011**, *115*, 17594–17598.

[42] J. D. Benck, B. A. Pinaud, Y. Gorlin, T. F. Jaramillo, *PLoS One* **2014**, *9*, e107942.

[43] C. M. H. Ferreira, I. S. S. Pinto, E. V Soares, H. M. V. M. Soares, *RSC Adv.* **2015**, *5*, 30989–31003.

[44] K. H. Scheller, T. H. J. Abel, P. E. Polanyi, P. K. Wenk, B. E. Fischer, H. Sigel, *Eur. J. Biochem.* **2018**, *107*, 455–466.

[45] C. D. Wagner, J. F. Moulder, L. E. R. Davis, W. M. Riggs, *Hand Book of X-Ray Photoelectron Spectroscopy*, **2008**.

[46] J. K. Heuer, J. F. Stubbins, *Corros. Sci.* **1999**, *41*, 1231–1243.

[47] K. J. Kyu, C. Yoonjun, J. M. Jin, L.-W. Ben, S. Dongguen, Y. Yeonjin, W. D. Hwan, Z. Xiaolin, P. J. Hyeok, *ChemSusChem* **2017**, *11*, 933–940.